

July 17, 2018

AN ANALYTIC MODEL FOR BUOYANCY RESONANCES IN PROTOPLANETARY DISKS

Stephen H. Lubow

Space Telescope Science Institute, 3700 San Martin Drive, Baltimore, MD 21218

lubow@stsci.edu

and

Zhaohuan Zhu¹*Department of Astrophysical Sciences, Princeton University, Princeton, NJ 08544*

zhzhu@astro.princeton.edu

ABSTRACT

Zhu, Stone, and Rafikov (2012) found in 3D shearing box simulations a new form of planet-disk interaction that they attributed to a vertical buoyancy resonance in the disk. We describe an analytic linear model for this interaction. We adopt a simplified model involving azimuthal forcing that produces the resonance and permits an analytic description of its structure. We derive an analytic expression for the buoyancy torque and show that the vertical torque distribution agrees well with results of Athena simulations and a Fourier method for linear numerical calculations carried out with the same forcing. The buoyancy resonance differs from the classic Lindblad and corotation resonances in that the resonance lies along tilted planes. Its width depends on damping effects and is independent of the gas sound speed. The resonance does not excite propagating waves. At a given large azimuthal wavenumber $k_y > h^{-1}$ (for disk thickness h), the buoyancy resonance exerts a torque over a region that lies radially closer to the corotation radius than the Lindblad resonance. Because the torque is localized to the region of excitation, it is potentially subject to the effects of nonlinear saturation. In addition, the torque can be reduced by the effects of radiative heat transfer between the resonant region and its surroundings. For each azimuthal wavenumber, the resonance establishes a large scale density wave pattern in a plane within the disk.

Subject headings: hydrodynamics – planet-disk interactions – stars: formation – stars: pre-main sequence – waves

¹Hubble Fellow

1. INTRODUCTION

Young planets can experience strong gravitational interactions with surrounding gas residing in a protoplanetary disk (Goldreich & Tremaine 1980; Lin & Papaloizou 1986; Ward 1997; Lubow & Ida 2011; Kley & Nelson 2012). These interactions can lead to structural changes in a disk through the launching of waves that can result in shocks and gap formation. They can also lead to changes in the orbital properties of the planet, resulting in their radial migration. Such phenomena are caused by the resonant forcing of the gas by the planet. The two types of resonances that describe this interaction, the Lindblad and corotational, have been extensively explored. Both of these resonances involve planar motions and will occur in a two-dimensional disk in which the vertical dynamical effects (perpendicular to the disk orbital plane) are ignored. For planets on circular orbits, the corotation resonance lies at the orbit of the planet. The gas response at the corotation resonance is of the form of a trapped radially evanescent wave with a radial drop-off on a scale of order the disk thickness h . The other form of resonance, the Lindblad resonance, occurs where a forcing frequency component due to the planet matches the epicyclic frequency of the gas. There are infinitely many of these resonances. In the absence of disk self-gravity, these resonances result in the launching of acoustic waves that transport energy and angular momentum away from the planet. The strongest Lindblad resonances lie close to the planet, but cannot occur closer than $\sim h$ radially from the orbit of the planet due to pressure effects.

When the disk vertical structure is taken into account, a richer set of waves can be excited at Lindblad resonances (Lubow & Ogilvie 1998; Bate et al. 2002). These waves are of the form of r modes (rotation-dominated), g modes (vertical buoyancy-dominated), p modes (pressure-dominated), and f modes (fundamental). For small or moderate azimuthal wavenumbers ($\ll h^{-1}$), the Lindblad response is dominated by an f mode, while the r-modes and g-modes are less strongly excited. In a vertically isothermal disk that undergoes adiabatic perturbations, as will be considered in this paper, the fundamental mode consists of two-dimensional planar motions.

By means of 3D shearing box simulations, Zhu et al (2012) have recently shown that a new form of planet-disk interaction can occur due to buoyancy resonances. For this type of resonance, the disk vertical motions play a critical role. At such a resonance, a planet forcing frequency component matches the free oscillation frequency of a vertically displaced fluid element that behaves adiabatically. Like the Lindblad case, there are infinitely many such resonances, one for each azimuthal wavenumber k_y . But since the free vertical oscillation frequency varies with height above the disk midplane, these resonances do not occur at particular radii as in the Lindblad case. Instead they lie along tilted planes. These resonances radially extend much closer to the planet than Lindblad resonances. The one-sided (inside or outside corotation) torque that results from the buoyancy resonances was found to be comparable to, but smaller than, the usual Lindblad torque.

The goal of this paper is to explore the analytic properties of buoyancy resonances. The analytic approach provides a verification of the existence of this resonance and insight into its structure. We consider the linear response of an isothermal disk that undergoes adiabatic perturbations to a

simplified form of forcing. As in Zhu et al (2012), we consider the gas to reside in a shearing box, as described in Section 2. We consider waves for which the azimuthal wavenumber is of order or greater than h^{-1} . These waves play an important role in determining the total torque caused by a planet. To make analytic progress, we consider forcing that is purely azimuthal and is independent of radius and height in the disk. In Section 3, we analyze a disk with constant vertical gravity and find separable solutions for the linear disk response. We obtain analytic expressions for the structure of the resonance and the torque distribution. We then consider in Section 4 the case of variable vertical gravity and determine the linear response numerically by means of a Fourier method in radius. We then show that the torque density in this case agrees well with the torque density obtained by an obvious extension of the torque density expression in the constant gravity case. Section 5 contains a discussion and Section 6 contains the summary.

2. LINEARIZED SHEARING BOX EQUATIONS

2.1. Basic Equations

We consider gas in a 3D shearing box described by Cartesian coordinates (x, y, z) in a frame that corotates with the disk at some radius r from the central star and generalize the 2D shearing sheet model (e.g., Goldreich & Tremaine 1978). The radial coordinate x is defined such that $x = 0$ occurs at radius r , and vertical coordinate z is defined such that $z = 0$ lies at the disk midplane. The disk has a characteristic thickness $h \ll r$. The unperturbed disk is taken to be isothermal with equation of state $p_0(z) = c^2 \rho_0(z)$ with isothermal sound speed c . The local angular speed of the disk is Ω and the unperturbed disk velocity in the corotating frame is $2Ax \mathbf{e}_y$, with constant shear rate $2A$.

We consider the effects of a single azimuthal Fourier component with azimuthal wavenumber $k_y > 0$ of the gravitational potential

$$\Psi(x, y, z) = \Phi(x, z) \exp(ik_y y). \quad (1)$$

We take $\Phi(x, z)$ to be real and thereby determine the phasing of $\Psi(x, y, z)$. We determine the y Fourier components of velocity (u, v, w) , density perturbation ρ , and pressure perturbation p as functions of x and z that describe the response to this potential. The linearized steady state shearing box equations for the x, y , and z motion, mass conservation, and heat for an adiabatic gas are respectively

$$2i Ak_y x u - 2\Omega v = -\partial_x \left(\frac{p}{\rho_0} + \Phi \right), \quad (2)$$

$$2i Ak_y x v + 2Bu = -ik_y \left(\frac{p}{\rho_0} + \Phi \right), \quad (3)$$

$$2i Ak_y x w = -g \frac{\rho}{\rho_0} - \frac{\partial_z p}{\rho_0} - \partial_z \Phi, \quad (4)$$

$$2i Ak_y x \rho + w \partial_z \rho_0 = -\rho_0 (\partial_x u + ik_y v + \partial_z w), \quad (5)$$

$$2i Ak_y x \left(\frac{p}{p_0} - \gamma \frac{\rho}{\rho_0} \right) = -w \partial_z \ln \left(\frac{p_0}{\rho_0^\gamma} \right) = -\frac{\gamma w N^2}{g}, \quad (6)$$

where $B = A + \Omega$ is an Oort constant, g is the vertical disk gravity that can generally be a function of z , and N is the vertical buoyancy frequency for gas that can also generally be a function of z

$$N(z) = \sqrt{\frac{\gamma - 1}{\gamma} \frac{g(z)}{c}}, \quad (7)$$

with adiabatic index γ .

Combining equation (4) for vertical motion with the heat equation (6), we have that the density perturbation is given by

$$\rho = -\frac{\gamma N^2 p_0 \partial_z p + \gamma \rho_0 p_0 N^2 \partial_z \Phi + 4A^2 k_y^2 x^2 \rho_0 g p}{\gamma g p_0 (N^2 - 4A^2 k_y^2 x^2)}. \quad (8)$$

The denominator on the right-hand side of equation (8) vanishes at a buoyancy resonance where the buoyancy frequency matches the forcing frequency

$$x_{\text{res}}(z) = \pm \frac{N(z)}{2Ak_y}. \quad (9)$$

The upper (lower) sign is appropriate for an inner (outer) buoyancy resonance, since A is negative. Equation (8) then contains possible singularities at buoyancy resonances.

2.2. Boundary Conditions

We describe here the boundary conditions that we generally apply. They are similar to those used in Zhu et al (2012). For an inner (outer) buoyancy resonance, we take the outer (inner) x boundary to be located at the corotation radius defined by $x = 0$. Near the $x = 0$ boundary, quantities are assumed to be point symmetric with respect to (x, y) . This condition means that

$$\text{Re}[p(x, z) \exp(ik_y y)] = \text{Re}[p(-x, z) \exp(-ik_y y)] \quad (10)$$

near $x = 0$. In its application to the boundary at $x = 0$, this relation implies $\text{Im}(p(0, z)) = 0$. A further application of equation (10) implies that $\text{Re}(\partial_x p(0, z)) = 0$. These conditions can be compactly written as

$$\text{Re}(\partial_x p(0, z)) + ik_y \text{Im}(p(0, z)) = 0. \quad (11)$$

For an inner (outer) buoyancy resonance, following Zhu et al (2012) we take the inner (outer) x boundary condition to be that the radial velocity perturbations vanish, $u = 0$. By combining equations (2) and (3), we obtain a condition on the pressure perturbation at this boundary that

$$\partial_x p = -\frac{A x \rho_0 \partial_x \Phi + \Omega \rho_0 \Phi + \Omega p}{A x}. \quad (12)$$

Periodic boundary conditions are applied in the y direction. This condition is automatically handled by our use of Fourier components in y .

In the z direction, we apply reflection boundary conditions at the disk midplane. That is,

$$w(x, 0) = 0. \quad (13)$$

This boundary condition implies that there is no mass flux through the disk midplane from above or below. Far from the disk midplane (large $|z|$), the disk pressure perturbations are assumed to vanish, $p = 0$.

2.3. Torque

To determine the torque due to a buoyancy resonance, we determine ρ near x_{res} . We assume, as we later show, that the numerator on the right-hand side of equation (8) does not vanish at a buoyancy resonance. We expand that equation about $x = x_{\text{res}}$ and obtain to lowest order that

$$\rho = \pm N \frac{\gamma p_0 \partial_z p + \gamma \rho_0 p_0 \partial_z \Phi + \rho_0 g p}{4\gamma g p_0 A k_y x'}, \quad (14)$$

where $x' = x - x_{\text{res}}$ is the x position relative to the resonance. To treat the singular behavior of ρ at $x' = 0$, we follow the standard procedure of extending x' to the complex plane and replacing x' by $x' + i l_d$ with small damping length l_d (e.g., Meyer-Vernet & Sicardy 1987). We then have that

$$\rho = \pm N \frac{\gamma p_0 \partial_z p + \gamma \rho_0 p_0 \partial_z \Phi + \rho_0 g p}{4\gamma g p_0 A k_y} \left[\frac{x'}{x'^2 + l_d^2} - \frac{i l_d}{x'^2 + l_d^2} \right]. \quad (15)$$

The second term in the brackets represents the "resonant" term that behaves as a Dirac delta function, since

$$\delta(x') = \frac{1}{\pi} \frac{l_d}{x'^2 + l_d^2} \quad (16)$$

for small l_d .

The torque density in z inside/outside corotation on the gas due to a particular y Fourier component of the perturbing potential Ψ is defined by

$$\frac{dT}{dz} = -r \int_{-\pi r}^{\pi r} \int_{x_i}^{x_o} \text{Re}[\rho(x, z) \exp(i k_y y)] \text{Re}[\partial_y \Psi(x, y, z)] dx dy \quad (17)$$

$$= -\pi r^2 k_y \int_{x_i}^{x_o} \text{Im}(\rho) \Phi dx, \quad (18)$$

where we used the fact that Φ is a real quantity in equation (1). The x integration limits apply either inside or outside corotation where x_i is the x inner boundary location and x_o is the x outer boundary location. For the case inside (outside) corotation, $x_o = 0$ ($x_i = 0$). We then obtain

$$\frac{dT}{dz} = \pm \frac{\pi^2 r^2 \Phi N}{4\gamma g p_0 A} (\gamma p_0 \text{Re}(\partial_z p) + \gamma \rho_0 p_0 \partial_z \Phi + \rho_0 g \text{Re}(p)), \quad (19)$$

where all x -dependent quantities are evaluated at the resonance where $x = x_{\text{res}}$. To evaluate the torque, we determine the pressure perturbation $p(x, z)$ near the resonance.

3. MODEL WITH CONSTANT VERTICAL GRAVITY AND SIMPLE AZIMUTHAL FORCING

3.1. Torque Derivation

In a standard thin disk, the buoyancy frequency N varies nearly linearly with z , due to the change in vertical gravity with z (see equation (7)). The resonance condition (9) is then satisfied along tilted planes. We simplify the geometry of the resonances by applying an approximate model for the vertical gravity. Above (below) the disk midplane, the vertical gravity is taken to be constant and downward (upward). In the analysis below, we consider the dynamics above the disk midplane where the downward vertical gravity is denoted by the constant $g > 0$. The resonance location simplifies to a vertical plane described by a particular value of x for each k_y . The constant vertical gravity model permits the dynamical equations to be separable in space and facilitates the development of an analytic model.

Vertical hydrostatic balance for constant gravity implies that the unperturbed disk satisfies

$$p_0(z) = p_{00} \exp(-|z|/h), \quad (20)$$

$$\rho_0(z) = \rho_{00} \exp(-|z|/h), \quad (21)$$

where

$$c^2 = gh, \quad (22)$$

with constants g , h , p_{00} and ρ_{00} . We also take

$$g = \Omega^2 h. \quad (23)$$

To make analytic progress, we adopt a simple potential of the form (1). We take the perturbing potential to be of the form

$$\Psi(x, y, z) = \Phi \exp(ik_y y), \quad (24)$$

where Φ on the right-hand side is a real constant. This potential gives rise to forcing that is purely azimuthal and is constant in x and z .

To investigate the nature of this simplification, we carried out some nonlinear numerical simulations using the Athena code. The simulations were of isothermal disks which are subject to various vertical gravities and undergo adiabatic perturbations caused by various potentials. We define dimensionless wavenumber and coordinates as $K_y = k_y h$, $X = x/h$ (a different X than defined in Section 3.2), $Y = y/h$, and $Z = z/h$. We express the perturbing potential in terms of the modified Bessel function K_0 . These simulations covered cases with

- (a) constant vertical gravity g and potential given by equation (24), so that $\Phi(X, Z) = C$,
- (b) variable vertical gravity and potential given by $\Psi(x, y, z) = C K_0(k_y x) \exp(ik_y y)$, so that $\Phi(X, Z) = C K_0(K_y X)$, and
- (c) variable vertical gravity and potential given by $\Psi(x, y, z) = C K_0(k_y \sqrt{x^2 + z^2}) \exp(ik_y y)$, so that $\Phi(X, Z) = C K_0(K_y \sqrt{X^2 + Y^2})$.

The disk structure and the potential perturbation become more realistic in going from Case (a) to (c).

Constant C is chosen as $5.8 \times 10^{-3} c^2$. For Case (c), this is equivalent to the k_y Fourier component of the potential of a planet with mass $5.8 \times 10^{-3} \pi M_* (h/r)^3$ or $0.76 M_\oplus$ with $h/r = 0.05$ and $M_* = M_\odot$. This value is sufficiently small that there is no gap opening. In Cases (b) and (c), a small smoothing length $5 \times 10^{-3} h$ has been used. A small isotropic viscosity has been used to resolve the resonance. The viscosity is $\nu = 10^{-6} \Omega h^2$ (or equivalently $\alpha = 10^{-6}$) for Case (a), while $\nu = 10^{-5} \Omega h^2$ (or equivalently $\alpha = 10^{-5}$) for Cases (b) and (c), respectively.

The simulated gas lies above the disk midplane $z > 0$ and outside corotation $x > 0$. The simulation setup was similar to that described in Zhu et al (2012). For Case (a), we used 32 vertical grid points per scale height that gives a total torque that is nearly independent of the resolution (the error is within 5%). However, the simulation does not resolve the vertical torque structure to very high accuracy. The peak of the torque density as a function of height z for the $k_y h = 2\pi$ mode is at $z \sim 0.2h$. For constant vertical gravity, we find that this resolution corresponds to about 6 vertical grid points near the peak of the torque density.

The boundary conditions follow those described in Section 2.2. The simulation domain and resolution (in x, y, z order) for these three simulations are respectively: (a) $(0, 0.3h) \times (-0.5h, 0.5h) \times (0, 5h)$ with the resolution of $252 \times 128 \times 640$, (b) $(0, 0.3h) \times (-0.5h, 0.5h) \times (0, 5h)$ with the resolution of $126 \times 64 \times 320$, and (c) $(0, 2h) \times (-0.5h, 0.5h) \times (0, 5h)$ with the resolution of $256 \times 64 \times 320$. In these simulations, we take $k_y h = 2\pi$ and $\gamma = 5/3$.

The simulations were conducted in dimensionless units with the dimensionless gas density ρ_s expressed in units of the unperturbed midplane density ρ_{00} , the dimensionless coordinates expressed in units of length h , and dimensionless time in units of Ω^{-1} . Accordingly, the dimensionless potential used in the simulations is $\Phi_s = \Phi/c^2$. From the simulation results, we determine the torque per length in the y direction that we multiply by $2\pi r$ to obtain the torque density $\partial_X \partial_Z T$. We expect the torque to scale with Φ^2 , since both the density perturbation and y gravitational force depend linearly on Φ . In Fig. 1, we plot the dimensionless torque density that is scaled by Φ_s^2 and is given by

$$\partial_X \partial_Z T_s = \frac{\pi K_y}{\Phi_s(X, Z)} \frac{1}{2Y_b} \int_{-Y_b}^{Y_b} \rho_s(X, Y, Z) \sin(K_y Y) dY, \quad (25)$$

where $\pm Y_b$ are the dimensionless locations of the y -boundaries of the simulations and ρ_s is the simulated disk density with both expressed in dimensionless units. This torque density is converted to the dimensional torque density $\partial_X \partial_Z T$ by multiplying by $r^2 h \rho_{00} \Phi^2(X, Z)/c^2$.

Fig. 1 provides some motivation for the gravity and potential simplifications. In all three Cases (a), (b), and (c), plotted in the respective panels after 7 orbits, the torque is confined to a narrow region centered on the buoyancy resonance. When scaled by $r^2 h \rho_{00} \Phi^2(X, Z)/c^2$, the torque densities have somewhat similar structures. The vertical orientation of the resonance in the case of constant gravity permits an analysis through separation of variables.

We concentrate on the case that k_y is large, $k_y \gtrsim h^{-1}$. We are interested in this regime because the total torque is dominated by contributions that occur at large k_y . The gas at resonance has sonic or subsonic unperturbed gas speeds at the resonance. Under such conditions, we expect the gas to respond approximately hydrostatically in the y direction, in order to prevent the development of rapid horizontal velocities u and v at large k_y (see equation (3)). That is,

$$p(x, z) = -\rho_0(z)\Phi \quad (26)$$

and p is a real function (in phase with real quantity Φ). We show that y -hydrostatic equation (26) is well satisfied for $k_y h \gg 1$ in Appendix A.

The torque density integral in equation (19) can then be readily evaluated. We use equation (26) to determine that

$$\frac{dT}{dz} = \pm \frac{\pi^2}{4} \frac{\gamma - 1}{\gamma} r^2 \rho_0(z) \Phi^2 \frac{N}{Ac^2} \quad (27)$$

or

$$\frac{dT}{dz} = \pm \frac{\pi^2}{4} r^2 \rho_0(z) \Phi^2 \frac{N^3}{Ag^2}. \quad (28)$$

Notice that the torque density is independent of the resonance width l_d and azimuthal wavenumber k_y , provided that k_y is large.

The torque density derivation assumed that the gas behaves hydrostatically in the azimuthal direction, equation (26). As discussed in Appendix B, this assumption breaks down in a region whose thickness is of order $1/k_y$ about the disk midplane, where the effects of the disk midplane boundary condition, equation (B), are important. This boundary condition requires the torque density dT/dz to vanish at the disk midplane. The resulting torque is given by equation (B5) of Appendix B.

3.2. Numerical Solution of Separable Equations

In Appendix A, we obtain a separable equation for the dimensionless pressure perturbation $P(X, Z) = p(X) \exp(-|Z|)/(\rho_{00}\Phi)$ off the midplane ($|z| > 1/k_y$, away from the influence of the $z = 0$ boundary), with $X = (x - x_{\text{res}})/h$ (a different X than defined in Section 3.1) and $Z = z/h$. We solve for pressure $P(X)$ given by equation (A4) numerically as a two point boundary value problem with the x boundary conditions that are described in Section 2.2. To determine this solution, we need to specify how to treat the singular $1/X$ term in the numerical integration across the

resonance. Following the procedure described in Section 2, we resolve the singularity by replacing $1/X$ by $1/(X + i\epsilon)$ where $0 < \epsilon \ll 1$ is a dimensionless length scale defined as $\epsilon = l_d/h$ that we choose to be $\epsilon = 1 \times 10^{-8}$. We adopt values for the adiabatic index $\gamma = 5/3$ and $K_y = k_y h = 5$. Fig. 2 plots the results for $P(X)$. Notice that the pressure perturbation $P(X)$ varies smoothly near the resonance, and its value there agrees well with the value of -1 predicted by the y -hydrostatic approximation (26), and as expected by the series solution (A10) for large K_y .

In Appendix A we determine the analytic properties of the buoyancy resonance. We verify them with the numerical solutions for the separable equations. Fig. 3 shows the behavior of the numerical solution for $P'(X)$ near the buoyancy resonance at $X = 0$. In agreement with the analytic calculation, equation (A15) of Appendix A, we see that there is a jump in the imaginary part of P' and a logarithmic singularity in the real part of P' . The dashed lines in Fig. 3 plot the analytic approximation to $P'(X)$ near the resonance and show good agreement.

Fig. 4 shows the behavior of the numerical solution for $P''(X)$ near the buoyancy resonance at $X = 0$. From equation (A12) of Appendix A, we expect $Im(P''(X))$ to be of the form of $\delta(X)$, for Dirac delta function δ , as is consistent with the plotted function. As discussed in Appendix A, this out of phase delta function contributes to the out of phase density response that in turn contributes to the localized torque at the resonance $X = 0$.

The leading variations in X for $|X| \ll 1$ and weak damping ($0 < \epsilon \ll 1$) of the various physical quantities at the buoyancy resonance for $K_y \gg 1$ and $|Z| \gg 1/K_y$ are given by

$$Re(u) \sim \arctan(X/\epsilon) \sim H(X), \quad (29)$$

$$Im(u) \sim \log(X^2 + \epsilon^2) \sim \log(|X|), \quad (30)$$

$$Re(v) \sim \log(X^2 + \epsilon^2) \sim \log(|X|), \quad (31)$$

$$Im(v) \sim \arctan(X/\epsilon) \sim H(X), \quad (32)$$

$$Re(w) \sim \frac{\epsilon}{X^2 + \epsilon^2} \sim \delta(X), \quad (33)$$

$$Im(w) \sim \frac{X}{X^2 + \epsilon^2} \sim 1/X, \quad (34)$$

$$Re(\rho) \sim \frac{X}{X^2 + \epsilon^2} \sim 1/X, \quad (35)$$

$$Im(\rho) \sim \frac{\epsilon}{X^2 + \epsilon^2} \sim \delta(X), \quad (36)$$

$$Re(p) \simeq -\rho_0 \Phi = -\rho_0 \Phi, \quad (37)$$

$$Im(p) \sim X + b_1 X \arctan(X/\epsilon) \sim X + b_2 X H(X), \quad (38)$$

where $H(X)$ is the Heaviside step function, b_i are real constants, and coefficients have been omitted in the \sim relations. The third column in equations (29) - (38) contains the functional forms in the limit of $\epsilon \rightarrow 0$ at fixed X .

Unlike the case of Lindblad resonances, there are no radially or vertically propagating waves launched. Unlike the case of the previously studied disk resonances, the resonance width in x is l_d

that is unrelated to the gas sound speed. The width is due to the effects of damping forces and radiative diffusion.

3.3. Comparison of Analytic Model With Simulations

Based on Athena simulation results, we determined the torque density dT/dZ for Case (a) that has constant Φ , as described in Section 3.1. Along the lines of equation (25), we calculated the dimensionless torque density dT_s/dZ for an outer resonance from the results of simulations by integrating the torque density in both the x and y directions at various heights Z above the disk midplane

$$\frac{dT_s}{dZ} = \frac{\pi K_y}{\Phi_s} \frac{1}{2Y_b} \int_{-Y_b}^{Y_b} \int_0^{X_b} \rho_s(X, Y, Z) \sin(K_y Y) dX dY, \quad (39)$$

where again ρ_s is the dimensionless gas density in units of the unperturbed midplane disk density ρ_{00} , $\Phi_s = \Phi/c^2$ is a dimensionless real constant, and X_b and $\pm Y_b$ are the dimensionless locations of the outer x boundary and both y boundaries of the simulations, respectively. The dimensional torque density dT/dZ is obtained by multiplying dT_s/dZ by $r^2 h \rho_{00} \Phi^2/c^2$. As seen in the Panel (a) of Fig. 1, the torque density was confined to a region of small radial extent centered on the buoyancy resonance. Fig. 5 compares the nonlinear simulation results for dT_s/dZ with predictions based on the analytic expression (B5) and shows good agreement.

4. MODEL WITH VARIABLE VERTICAL GRAVITY AND SIMPLE AZIMUTHAL FORCING

4.1. Torque

We extend the constant gravity and simple potential model of Section 3 to the more realistic case in which the vertical gravity varies linearly in z , as expected in a thin disk. We apply the simple potential given by equation (24). Vertical hydrostatic balance implies that the unperturbed disk satisfies

$$p_0(z) = p_{00} \exp(-z^2/(2h^2)), \quad (40)$$

$$\rho_0(z) = \rho_{00} \exp(-z^2/(2h^2)), \quad (41)$$

where

$$h = c/\Omega \quad (42)$$

with constants c , h , p_{00} , and $\rho_{00} = p_{00}/c^2$. We also have

$$g(z) = \Omega^2 z \quad (43)$$

and

$$N(z) = \sqrt{\frac{\gamma-1}{\gamma}} \Omega \frac{|z|}{h}. \quad (44)$$

Based on the torque density expression (28), we postulate that the torque in the variable gravity case is given by

$$\frac{dT}{dz} = \pm \frac{\pi^2}{4} r^2 \rho_0(z) \Phi^2 \frac{N^3(z)}{A g^2(z)}. \quad (45)$$

This torque density expression follows from the application hydrostatic condition (26) to the torque equation (19) with variable gravity. For small z , the torque density varies linearly with z .

The integrated buoyancy torque for each $k_y > 1/h$ is then given by

$$T = \pm \frac{\sqrt{2}\pi^{3/2}}{4} \left(\frac{\gamma-1}{\gamma}\right)^{3/2} \left(\frac{r}{h}\right)^2 \Sigma \frac{\Phi^2}{A\Omega}, \quad (46)$$

independent of k_y . The Lindblad torque has a much different dependence on wavenumber k_y . We compare the buoyancy torque T to the Lindblad torque T_L subject to the same potential given by equation (24). We consider wavenumbers near the torque cutoff, $k_y r \sim r/h \gg 1$ and have that

$$T_L = \mp \frac{4\pi^2 k_y^2 r^2 \Sigma \Phi^2}{3\Omega^2}, \quad (47)$$

which follows from equation (13) of Goldreich & Tremaine (1980) for a Keplerian disk.

The ratio of the torques in a Keplerian disk with $\gamma = 5/3$ is given by

$$\frac{T_L}{T} = 5\sqrt{5\pi}(k_y h)^2 \simeq 20(k_y h)^2. \quad (48)$$

Since we are considering wavenumbers with $k_y h \sim 1$, we see that the Lindblad torque is much stronger.

Zhu et al (2012) reported that the one-sided (inside or outside corotation) total buoyancy torque in the case of the planet potential was tens of percent of the one-sided total Lindblad torque and was then much stronger in a relative sense than suggest by equation (48). This difference is likely due to the use here of a potential that is independent of x and z . The buoyancy torque in the point mass case may be getting stronger potential contributions that lie closer to the planet than the Lindblad torque. In addition, the Lindblad torque declines above its torque cutoff, for $k_y \gtrsim 1/h$. In the point mass case, the Lindblad and buoyancy torques likely vary differently with k_y for wavenumbers above the Lindblad torque cutoff. Such differences may explain why the buoyancy torque (integrated over k_y) is relatively stronger in the point mass case than the estimate here suggests.

4.2. Linear Numerical Calculation

In Section 3.3 we showed that the torque obtained by linear theory agrees well with that determined by nonlinear simulations. Unlike the constant vertical gravity case described in Section 3.2, we cannot obtain separable solutions to the linearized equations. Instead, we determine the torque in the variable gravity case through a numerical solution to the linearized equations by means of a Fourier method in x . This method is a 3D extension of the sheared coordinate approach taken by Goldreich & Tremaine (1978). We describe the method in Appendix C.

Equations (C4) - (C8) describe the dynamics in terms of the x Fourier transforms of physical quantities $q(x, z)$ to quantities $\hat{q}(\tau, z)$. The equations are expressed in terms of a time-like coordinate τ and vertical coordinate z . These equations were nondimensionalized by setting $\Omega = 1$, $h = 1$, $\rho_{00} = 1$ and following the dimensionless variable notation of Section 3.1. We integrated these equations by means of the Method of Lines in Mathematica with the implicit Runge-Kutta option for various values of K_y using $\nu_w = 0.001$, $\hat{\Phi} = 0$ (see explanation above equation (C23)). The integration extended from $\tau = \tau_s = 0$ to $\tau = \tau_f = 140/\sqrt{K_y}$ and Z from 0 to 4. Boundary conditions (C23) - (C30) were applied with $\Phi = 1$. The results were transformed back to $q(X, Z)$ and the torque density, normalized by $r^2 h \rho_{00} \Phi^2 / c^2$, was determined from the integral

$$\frac{dT}{dZ} = -\pi K_y \int_0^{X_o} \text{Im}(\rho(X, Z)) dX \quad (49)$$

in dimensionless units. The width of the peak in the density profile in X in the numerical calculation is determined mainly by the length of the τ integration, τ_f . The upper limit of the torque integral X_o was typically chosen to be $2X_{\text{res}}$ that is far enough away from the resonance that the resonant density perturbation is small.

In Fig. 6 we compare the results of this calculation with the torque density equation (45) for cases with $K_y = 5$ and 10 and $\gamma = 5/3$. As expected, the torque distribution is independent of K_y for this potential. The agreement is very good.

5. DISCUSSION

Buoyancy resonances have been previously analyzed in the context of high mass stars that are tidally perturbed by a companion (Zahn 1975; Goldreich & Nicholson 1989). A buoyancy resonance occurs near the outer parts of the stellar convective core where the buoyancy frequency changes from low values in the core to high values in the radiative envelope. Within this region, the buoyancy frequency matches that of the tidal forcing. The response of the star is to launch buoyancy waves (g mode waves) that propagate towards the stellar surface where the waves damp and act to bring about spin synchronization with the binary orbit.

As we see in this paper, the adiabatic response of a disk to tidal forcing is evidently quite different. In the axisymmetric case of an isothermal disk, buoyancy waves (g modes) can be excited

at a Lindblad resonance (Bate et al. 2002). They propagate on the same side of the Lindblad resonance as the fundamental mode propagates which is not the region where the buoyancy resonance discussed here is found. For a vertically truncated isothermal disk, they accumulate near the disk upper boundary. We do not find evidence for these waves in the numerical results presented here at small $|x| < h$.

Low frequency axisymmetric waves in the form of r (rotation-dominated) modes exist and are affected by buoyancy that confines them near the disk midplane (see Fig. 11 of Lubow & Pringle (1993)). These modes can also be excited at a Lindblad resonance and propagate toward corotation ($x = 0$), although they are only weakly excited there (Bate et al. 2002).

To understand the star-disk difference, consider low frequency modes of given k_y in the region where wave frequency $|\omega|$ is smaller than epicyclic frequency κ , which is the region where the buoyancy resonances described in this paper reside. In a region such that $k_y \ll |k_x|$, the WKB dispersion relation for the disk pressure perturbation is

$$k_x^2 = \frac{\kappa^2 - \omega^2}{\omega^2 - N^2(z)} k_z^2, \quad (50)$$

where ω is the wave frequency and

$$\omega = 2Ak_y x \quad (51)$$

(Vishniac et al. 1990; Goodman 1993). This relation can be easily derived from equation (A1). We see then from equation (50) that vertical propagation is possible ($k_z^2 > 0$) only for low values of the buoyancy frequency, $N^2 < \omega^2$. For a disk with $N \propto z$, such a wave can propagate vertically only in the region near the disk midplane as an r mode.

Consider the stellar case. To see how waves can be launched towards a stellar surface, we adapt equation (50) to the case of a star by noticing that k_z in a disk describes phase variations along the direction of the buoyancy gradient. In the case of a star, the buoyancy gradient is in the (spherical) radial direction, and so we identify k_z with k_r . We identify the square of the wavenumber perpendicular to the buoyancy gradient with $k_x^2 \sim \ell(\ell + 1)/r^2$ for the spherical harmonic of order ℓ that is associated with the tidal field. We disregard the stellar rotation and set $\kappa = 0$. The tidal forcing frequency due to the companion star is ω . We then have that

$$k_r^2 = \frac{\ell(\ell + 1)}{r^2} \frac{N^2 - \omega^2}{\omega^2}. \quad (52)$$

Radial wave propagation is possible (i.e., $k_r^2 > 0$) in the radiative outer layers of a star outside the buoyancy resonance where $N^2(r) > \omega^2$ (cf. equation (15) of Goldreich & Nicholson (1989) with $\ell = 2$). Waves can be launched at the resonance where $N^2(r) \simeq \omega^2$ because the long wavelength of the wave $\sim 1/k_r$ can match the spatial scale of the slowly varying tidal field. The effects of rotation modify the dispersion relation by changing ω^2 in the denominator on the right-hand side of equation (52) to $\omega^2 - \kappa^2$. Therefore, one major difference between the disk case investigated here and stellar case is due to the effects of rapid rotation, κ , in the low frequency disk case.

Consider possibility that r modes are launched at buoyancy resonances in disks. Waves are launched at resonances if there is a strong overlap between the spatial form of the wave with that of the forcing. Typically that occurs at wave turning points where the long wavelength form of the wave matches the form of the relatively slowly varying potential. For example, from equation (50), k_x is small near a Lindblad resonance where $\omega = \pm\kappa$. This locally long wavelength permits a strong coupling with the tidal potential that results in the excitation of a wave. Although vertical wave turning points for r modes lie on the buoyancy resonance plane ($k_z = 0$ at $\omega = N$ in equation (50)), the radial wavenumbers k_x are large, as follows from equation (58) of Lubow & Pringle (1993) with dimensionless frequency $F = 2Axk_y/\Omega$ for $|F| \ll 1$. (Note: Lubow & Pringle (1993) used the term g modes for what are r modes, see also Ogilvie (1998).) The r mode becomes more confined vertically as it approaches corotation. Its vertical wavenumber k_z at the midplane and radial wavenumber k_x both grow to very large values near corotation ($x = 0$). Therefore, the r mode structure may not generally match the spatial form of the potential along the buoyancy resonance. This lack of matching may explain why r modes are not excited at buoyancy resonances.

Differential equation (A4), which we obtained for the pressure perturbation near a buoyancy resonance in the constant gravity case, is consistent with dispersion relation (50). In that case, N is constant, $k_z^2 = -1/h^2$ (see equation (A2)), and near the buoyancy resonance $N^2 - \omega^2 \propto x - x_{\text{res}} \propto X$. We then have that $k_x^2 \propto 1/X$ which covers the leading order terms on the left-hand side of equation (A4), identifying $P''(X)$ with $-k_x^2 P(x)$. However, the WKB approximation does not provide much insight into the properties of a buoyancy resonance because it does not involve waves.

Lubow & Pringle (1993) determined the structure of the disk modes by using what could be called the "waveguide" model. In that model, the amplitude variations in the x direction are assumed to occur slowly compared to phase variations. For perturbations induced by the buoyancy resonance, that assumption does not apply. For the case of vertically varying gravity, amplitude variations along both the x and z directions are rapid and comparable.

6. SUMMARY

The interaction between a planet and a disk that responds adiabatically can be understood qualitatively in terms of a 3D impulse delivered to the gas as it passes by the vicinity of the planet (Zhu et al 2012). The impulse generates a wake whose density is affected by the buoyancy of the gas. The wake in turn causes a planet-disk torque.

To understand the physical nature of the response of the gas, we have examined its nonaxisymmetric response to a potential that has a single azimuthal wavenumber k_y . We analyzed the role of buoyancy resonances in a disk whose unperturbed vertical structure is isothermal and is subject to adiabatic perturbations. A vertically displaced fluid element undergoes vertical free oscillations at the buoyancy frequency N . Although the gravitational forcing we have adopted was simplified to be purely azimuthal, this forcing induces nonaxisymmetric vertical pressure and buoyancy forces

with azimuthal wavenumber k_y that are stationary in the frame of the potential. Fluid elements move azimuthally through this vertical force field at velocity $2Ax$ due to the disk shear. The vertical forcing frequency on the fluid elements is then $2Axk_y$. A buoyancy resonance occurs where the absolute values of the free (N) and forcing frequencies ($2Axk_y$) match, as given by equation (9). The resonance leads to a nonaxisymmetric density response that contains a contribution that is out of phase with respect to the potential and results in a torque.

To carry out the analysis, we first considered the case of a disk with constant vertical gravity that is subject to a simple perturbing potential given by equation (24). The resonance in this case lies along a plane that is perpendicular to the disk plane, at some x_{res} (independent of z) given by equation (9). We obtained an analytic linear description of the structure of the resonance. The effects on the gas are highly localized to the plane of the resonance. The results show that the localized induced motions cause localized density perturbations and a torque (see Fig. 5). This result confirms the existence of the buoyancy torque found in simulations by Zhu et al (2012).

The pressure perturbation is everywhere smooth, but singular behavior occurs in its second radial derivative that leads to a contribution to the torque (Figs. 2 - 4) from the radial derivative of the radial velocity. The width of the torque region is controlled by damping processes and not gas pressure. The resonance does not result in radially or vertically propagating waves.

We then considered the case of variable vertical gravity with the same simple perturbing potential. Unlike the case of disk resonances previously studied, the buoyancy resonances in this case lie on tilted planes $x_{\text{res}} \propto z$. We obtained an analytic formula for the torque density, equation (28) that agrees well with numerical calculations (see Fig. 6). The buoyancy resonance exerts a torque over a region that lies radially closer to the corotation radius than the Lindblad resonance.

Buoyancy resonances have then very different properties from Lindblad resonances. They do not result in vertically or horizontally propagating waves. Their width is not determined by the gas sound speed, but instead by damping.

The current analysis has several limitations that could be overcome in future studies. The potential was taken to be of a very simple form in order to investigate the existence and basic analytic properties of a buoyancy resonance. But a more realistic potential would provide a more accurate description in a linearized model. The analysis presented here assumed that the gas behaves adiabatically. The radiative transfer of heat between the resonant region and its surroundings can reduce the buoyancy force on perturbed gas and so weaken the resonance for sufficiently low values of the disk optical depth. In addition, this heat exchange plays a role in determining the resonance width.

Since the torque is confined to a thin layer, the resonance may saturate (weaken) by feedback effects that may act to change the local disk structure. Such effects cannot be studied by linear theory. The analysis thus far has been limited to shearing boxes. The shearing box does not describe the corotation resonance and its possible interaction with the buoyancy resonance. The effects of the buoyancy torque on the net migration rate and in particular its direction (inwards

or outwards) depend on a competition between the inner and outer buoyancy torques that in turn depends on gradients of disk parameters. The determination of the outcome requires going beyond the shearing box approximation.

We benefitted from useful discussions with Gordon Ogilvie, Roman Rafikov, and Jim Stone. SHL acknowledges support from NASA Origins grant NNX11AK61G. ZZ acknowledges support by NASA through Hubble Fellowship grant HST-HF-51333.01-A awarded by the Space Telescope Science Institute, which is operated by the Association of Universities for Research in Astronomy, Inc., for NASA, under contract NAS 5-26555. All simulations were carried out using computers supported by the Princeton Institute of Computational Science and Engineering and Kraken at National Institute for Computational Sciences through XSEDE grant TG-AST130002.

A. PRESSURE PERTURBATION FOR CONSTANT VERTICAL GRAVITY AND SIMPLE AZIMUTHAL FORCING

We examine the behavior of pressure near the buoyancy resonance and verify the y -hydrostatic approximation of equation (26) for the perturbing potential of the form given by equation (24) in the limit of $k_y h \gg 1$. Above the disk midplane, for a given k_y , the gas dynamical equations (2) - (6), together with equations (20) and (21), can be combined to provide a single equation for the pressure perturbation p that is given by

$$\begin{aligned} & \frac{\kappa^2 - (2Ak_y x)^2}{(2Ak_y x)^2 - N^2} \left(\partial_z^2 p + \frac{\partial_z p}{h} + \frac{p(\gamma - 1)}{\gamma^2 h^2} \right) \\ = & \partial_x^2 p + \partial_x p \frac{8A^2 k_y^2 x}{\kappa^2 - (2Ak_y x)^2} + p \left(\frac{8A\Omega k_y^2}{\kappa^2 - (2Ak_y x)^2} - k_y^2 - \frac{(\kappa^2 - (2Ak_y x)^2)}{\gamma c^2} \right) \\ & + k_y^2 \rho_0(z) \Phi \left(\frac{8A\Omega}{\kappa^2 - (2Ak_y x)^2} - 1 \right). \end{aligned} \quad (\text{A1})$$

For the case of constant vertical gravity above the disk midplane and the simple potential given by equation (24), equation (A1) is separable in x and z . The pressure perturbation is of the form

$$p(x, z) = p(x) \exp(-|z|/h). \quad (\text{A2})$$

We apply a change to dimensionless variables

$$\begin{aligned} X &= \frac{x - x_{\text{res}}}{h}, \\ Z &= \frac{z}{h}, \\ P(X) &= \frac{p(X)}{\rho_{00} \Phi}, \\ K_y &= k_y h \end{aligned} \quad (\text{A3})$$

and obtain an ordinary differential equation of the form

$$s_2(X) P''(X) + s_1(X) P'(X) + s_0(X) \frac{P(X)}{X} = s_3(X), \quad (\text{A4})$$

where $s_i(X)$ are real polynomials in X that are nonzero at the resonance, that is $s_i(0) \neq 0$.

Close to the buoyancy resonance (small $|X|$), there is a $1/X$ singularity multiplying $P(X)$. We expect this term to balance the term involving the highest order derivative in X , that is $P''(X)$. The reason is that this highest derivative term is most sensitive to the structure of $P(X)$. If we assume that $P''(X) \sim O(1/X)$, then $P \sim O(X \log X)$ for $X > 0$. We then consider the following series for $P(X)$ for small $X > 0$,

$$P(X) = c_0 + (c_1 X + c_2 X^2) \log(X) + d_1 X + d_2 X^2, \quad (\text{A5})$$

where c_i and d_i are coefficients to be determined. We neglect higher order terms in X . Notice that p is smooth in X and $\lim_{X \rightarrow 0^+} P = c_0$. The first derivative of P contains a logarithmic singularity and its second derivative contains a $1/X$ singularity at $X = 0$.

Substituting expansion (A5) into equation (A4) for P , we obtain in lowest order (order $1/X$) an equation of the form

$$c_0 = a_1 c_1, \quad (\text{A6})$$

where a_i used here and below are constant terms that depend on A , κ , N , and Ω . In next order, we obtain an equation of the form

$$c_0 + a_2 + a_3 c_1 + a_4 c_2 + a_5 d_1 + a_6 d_2 + (a_7 c_1 + a_8 c_2) \log(X) = 0, \quad (\text{A7})$$

where a_2 arises from the inhomogeneous term. We then require the coefficient of $\log(X)$ to vanish and the sum of the other terms to vanish. Namely,

$$c_0 + a_2 + a_3 c_1 + a_4 c_2 + a_5 d_1 + a_6 d_2 = 0 \quad (\text{A8})$$

and

$$a_7 c_1 + a_8 c_2 = 0. \quad (\text{A9})$$

We then solve the three equations (A6), (A8), and (A9) for three unknowns c_0 , c_1 , and c_2 in terms of d_1 and d_2 . These two d_i parameters are due to the two boundary conditions in X for this second order equation in X .

In the limit of large K_y or equivalently small $X_{\text{res}} = x_{\text{res}}/h$, we find

$$c_0 = \frac{p(x_{\text{res}})}{\rho_{00} \Phi} = -1 + K_y^{-1} q_1 d_1 + K_y^{-2} q_2 (d_2 + q_3) + O(K_y^{-3}) \quad (\text{A10})$$

where q_i are dimensionless order unity coefficients that depend on A , κ , N , and Ω . In the large K_y limit, we expect the terms on the right-hand side of equation (A10) involving K_y to vanish. In this

limit, equation (A10) then implies equation (26) that in turn implies the torque given by equation (28). In practice, we find that the coefficient of the K_y^{-1} is typically small.

Notice that we are assuming that the d_i terms do not increase substantially with K_y . To do so would imply that the pressure perturbation varies by substantial amounts over the distance between resonance and corotation that varies inversely with K_y . For smooth solutions, the terms in equation (A10) involving d_i can be ignored in for large K_y . The smoothness condition on $Re(p)$ that determines the torque (see equation (19)) is expected hold as a consequence of the x boundary condition (11).

The series solution for $X < 0$ follows similarly, however, there is a jump in P' across the resonance. The imaginary part of P' undergoes a jump in value, as can be seen by integrating equation (A4) in a small region about $X = 0$

$$s_2(0) \int_{0^-}^{0^+} P''(X) dX = s_2(0) P'(X)|_{0^-}^{0^+} = s_0(0) \int_C \frac{P(0)}{X} dX = i \pi P(0) s_0(0), \quad (\text{A11})$$

where we have taken the integral along a counterclockwise contour C that is a small half circle in the upper half-plane about the $1/X$ pole (Meyer-Vernet & Sicardy 1987). The expansion for P that is valid for small positive and negative X values can then be written as

$$P(X) = c_0 + (c_1 X + c_2 X^2) \log |X| + i c_3 H(-X) X + d_1 X + d_2 X^2, \quad (\text{A12})$$

where H is the Heaviside step function and

$$c_3 = -\frac{\pi P(0) s_0(0)}{s_2(0)} \quad (\text{A13})$$

$$\simeq \frac{\pi s_0(0)}{s_2(0)}, \quad (\text{A14})$$

where we have used the fact that $P(0) = c_0 \simeq -1$ for large K_y , as seen in equation (A10), in obtaining the last equation. It can be shown that c_i are real for large K_y .

Having determined the form of the pressure near the resonance, we can determine leading singular behavior of the velocities from equations (2) - (6). As follows from equation (A12), near the buoyancy resonance $X = 0$,

$$P'(X) \sim c_1(1 + \log |X|) + i c_3 H(-X) + d_1. \quad (\text{A15})$$

To lowest order in K_y^{-1} for a Keplerian disk, quantity c_1 is given by

$$c_1 = -\frac{\sqrt{\gamma - 1}}{3\gamma^{5/2} K_y}. \quad (\text{A16})$$

We find that $u \sim i k_1 P'(X)$, $v \sim k_2 P'(X)$, $w \sim k_3 \delta(X)$ near $X = 0$ for real constants k_i and Dirac delta function $\delta(X)$. Consequently, u and v are logarithmically singular near the resonance. The equation of mass conservation (5) implies that $Im(\rho) \sim k_4 u'(X) + k_5 w(X) \sim k_6 \delta(X)$. This out of phase mass density contribution then leads to the local resonant torque density.

B. TORQUE MODIFICATION DUE TO MIDPLANE BOUNDARY CONDITION FOR CONSTANT VERTICAL GRAVITY

The torque derivation that led to equation (28) ignored the effects of the boundary conditions at the disk midplane discussed in Section 2.2. We consider here the effects of the midplane boundary condition that we take as $w(x, 0) = 0$, equation (B). For $X > 0$, we determine homogenous solutions for the pressure perturbation of the form

$$p_h(X, Z) = [1 + (c_1 X + c_2 X^2) \log(X) + d_1 X + d_2 X^2] \exp(-\lambda Z), \quad (\text{B1})$$

where λ is a dimensionless constant that is to be determined. Solutions to the linearized pressure perturbation equation can be obtained as in the inhomogeneous case of Appendix A. In the homogeneous case, c_0 does not appear because the solution has an arbitrary scale factor. Instead, the expanded pressure equations are solved for λ , c_1 , and c_2 . In the limit of large K_y , these equations imply that

$$\lambda = \frac{2k_y h \sqrt{a}}{\sqrt{3}(\kappa^2 - N^2)}, \quad (\text{B2})$$

where

$$a = -A \left[A(N^2 + \kappa^2) + \sqrt{A^2(N^2 + \kappa^2)^2 + 6N^2(\kappa^2 - N^2)(\kappa^2 - 8A\Omega - N^2)} \right]. \quad (\text{B3})$$

For a Keplerian disk with $\gamma = 5/3$, the above evaluates to $\lambda \simeq 2.5k_y h$.

Near the resonance, the vertical velocity and density perturbation are simply related by

$$\rho(X, Z) = \mp \frac{i\rho_0 N}{g} w(X, Z). \quad (\text{B4})$$

Consequently, the requirement that $w = 0$ at the disk midplane implies that ρ and therefore the torque density dT/dz also vanish there. The equation for the density perturbation variation in Z and thus dT/dz are modified by an additional term that is a homogeneous solution with Z variation $\exp(-\lambda|Z|)$ to account for this boundary condition. The resonant torque distribution in z is then given by

$$\frac{dT}{dz} = \pm \frac{\pi^2}{4} r^2 \rho_{00} \Phi^2 \frac{N^3}{A g^2} [\exp(-|z|/h) - \exp(-\lambda|z|/h)] \quad (\text{B5})$$

with λ given by equation (B2).

C. SHEARING BOX CALCULATION WITH VARIABLE GRAVITY

Equations (2) - (6) can be solved by applying a Fourier method to the x coordinate through the use of sheared coordinates as described in Goldreich & Tremaine (1978); Goldreich & Tremaine (1980). We added a viscous term $\nu_w \partial_z^2 w$ to the right-hand side of equation (4) to provide greater stability for the numerical scheme. The z coordinate is not transformed.

The Fourier transformations are

$$\hat{q}(\tau, z) = \frac{1}{2\pi} \int_{-\infty}^{\infty} q(x, z) \exp(-ik_y \tau x) dx, \quad (\text{C1})$$

where q is Φ , u , v , w , ρ , or p and

$$\tau = k_x/k_y - 2At. \quad (\text{C2})$$

The inverse transformations are given by

$$q(x, z) = k_y \int_{\tau_s}^{\tau_f} \hat{q}(\tau, z) \exp(ik_y \tau x) d\tau. \quad (\text{C3})$$

The limits of integration should ideally extend to $\tau_s = -\infty$, and $\tau_f = \infty$. In the numerical scheme, they are of course limited.

The transformed dynamical equations (2) - (6) are respectively

$$\partial_\tau \hat{u} - 2\tilde{\Omega} \hat{v} = -ik\tau \left(\frac{\hat{p}}{\rho_0} + \hat{\Phi} \right), \quad (\text{C4})$$

$$\partial_\tau \hat{v} + 2\tilde{B} \hat{u} = -ik \left(\frac{\hat{p}}{\rho_0} + \hat{\Phi} \right), \quad (\text{C5})$$

$$-2A \partial_\tau \hat{w} = -g \frac{\hat{p}}{\rho_0} - \frac{\partial_z \hat{p}}{\rho_0} - \partial_z \hat{\Phi} + \nu_w \partial_z^2 \hat{w}, \quad (\text{C6})$$

$$\partial_\tau \hat{\rho} - \frac{1}{2A} \hat{w} \partial_z \rho_0 = -\rho_0 \left(ik\tau \hat{u} + ik\hat{v} - \frac{1}{2A} \partial_z \hat{w} \right), \quad (\text{C7})$$

$$\partial_\tau \left(\frac{\hat{p}}{c^2} - \gamma \hat{\rho} \right) = \frac{\rho_0 \hat{w} (\gamma - 1)}{2A} \frac{z}{h^2}, \quad (\text{C8})$$

where

$$\tilde{\Omega} = -\frac{\Omega}{2A}, \quad (\text{C9})$$

$$\tilde{B} = -\frac{B}{2A}, \quad (\text{C10})$$

$$k = -\frac{k_y}{2A}. \quad (\text{C11})$$

$$(\text{C12})$$

These are partial differential equations with a time-like coordinate τ and a spatial coordinate z . Guided by Section 2.2, we apply the following boundary conditions at the disk midplane and upper boundary z_u

$$\hat{w}(\tau, z = 0) = 0, \quad (\text{C13})$$

$$\hat{p}(\tau, z = z_u) = 0, \quad (\text{C14})$$

$$\hat{w}(\tau, z = z_u) = 0. \quad (\text{C15})$$

We consider the simple potential in which $\Phi(x, z)$ is real constant (equation (24)).

$$\hat{\Phi}(\tau, z) = \frac{1}{2\pi} \int \Phi \exp(-ik_y \tau x) dx \quad (\text{C16})$$

$$= \frac{\Phi}{k_y} \delta(\tau). \quad (\text{C17})$$

Since the potential turns on at $\tau = 0$, we assume that for $\tau < 0$, all perturbed quantities are zero, e.g., $\hat{q} = 0$. We integrate the above equations over a very short interval centered at $\tau = 0$ and obtain

$$\hat{u}(0+, z) = 0, \quad (\text{C18})$$

$$\hat{v}(0+, z) = \frac{i\Phi}{2A}, \quad (\text{C19})$$

$$\hat{w}(0+, z) = 0, \quad (\text{C20})$$

$$\hat{\rho}(0+, z) = 0, \quad (\text{C21})$$

$$\hat{p}(0+, z) = 0. \quad (\text{C22})$$

We then we integrate equations (C4) - (C8) in τ starting with $\tau = 0$, subject to the initial conditions (C18) - (C22) with $\hat{\Phi} = 0$ (homogeneous equations).

We apply the following boundary conditions

$$\hat{u}(0, z) = 0, \quad (\text{C23})$$

$$\hat{v}(0, z) = \frac{i\Phi}{2A}, \quad (\text{C24})$$

$$\hat{w}(0, z) = 0, \quad (\text{C25})$$

$$\hat{\rho}(0, z) = 0, \quad (\text{C26})$$

$$\hat{p}(0, z) = 0, \quad (\text{C27})$$

$$\hat{w}(\tau, 0) = 0, \quad (\text{C28})$$

$$\hat{w}(\tau, z_u) = 0, \quad (\text{C29})$$

$$\hat{p}(\tau, z_u) = 0. \quad (\text{C30})$$

We need to obtain the density perturbation $\rho(x, z)$ in order to determine the torque distribution. The inverse Fourier transform (C3) contains artificial, small amplitude, rapid oscillations of density in x , due to the finite duration of $\hat{\rho}$ to $\tau = \tau_f$ and the lack of its periodicity over this interval. To remove these unwanted oscillations, we multiply $\hat{\rho}(\tau, z)$ by a window (or tapering) function that drops to nearly zero at τ_f (e.g., Press et al. (1992)). The window function was taken to be a Gaussian that is then applied to the density as

$$\rho(x, z) = k_y \int_0^{\tau_f} \hat{\rho}(\tau, z) \exp(-4(\tau/\tau_f)^2) \exp(ik_y \tau x) d\tau. \quad (\text{C31})$$

This procedure eliminated the unwanted oscillations. It gives similar results to those obtained by applying sufficiently strong viscous damping in the radial and azimuthal dynamical equations (C4) and (C5), respectively. Fast Fourier transforms were applied in Mathematica to evaluate the integral in equation (C31).

In Fourier space, the outer buoyancy torque produces low frequency oscillations in τ corresponding to a density disturbance at small $0 < x < h$. Since an outer Lindblad resonance wave occurs further out in x , it produces higher frequency disturbances in τ . Determining the properties of the buoyancy resonance then involves separating the low from high frequency signals.

REFERENCES

- Bate, M. R., Ogilvie, G. I., Lubow, S. H., & Pringle, J. E. 2002, *MNRAS*, 332, 575
- Goldreich, P., & Nicholson, P. D. 1989, *ApJ*, 342, 1079
- Goldreich, P., & Tremaine, S. 1978, *ApJ*, 222, 850
- Goldreich, P. & Tremaine, S. 1980, *ApJ*, 241, 425
- Goodman, J. 1993, *ApJ*, 406, 596
- Kley, W., & Nelson, R. P. 2012, *ARA&A*, 50, 211
- Lin, D. N. C., & Papaloizou, J. 1986, *ApJ*, 309, 846
- Lubow, S.H., Pringle, J.E., 1993, *ApJ*, 409, 360
- Lubow, S. H., & Ogilvie, G. I. 1998, *ApJ*, 504, 983
- Lubow, S. H., & Ida, S. 2011, *Exoplanets*, edited by S. Seager. Tucson, AZ: University of Arizona Press, 2011, 526 pp. ISBN 978-0-8165-2945-2., p.347-371
- Meyer-Vernet, N.& Sicardy, B., 1987, *Icarus*, 69, 157
- Ogilvie, G. I. 1998, *MNRAS*, 297, 291
- Press, W. H., Teukolsky, S. A., Vetterling, W. T., & Flannery, B. P. 1992, Cambridge: University Press, —c1992, 2nd ed.,
- Vishniac, E. T., Jin, L., & Diamond, P. 1990, *ApJ*, 365, 648
- Ward, W. R. 1997, *ApJ*, 482, L211
- Zahn, J.-P. 1975, *A&A*, 41, 329
- Zhu, Z., Stone, J. M., & Rafikov, R. R. 2012, *ApJ*, 758, L42

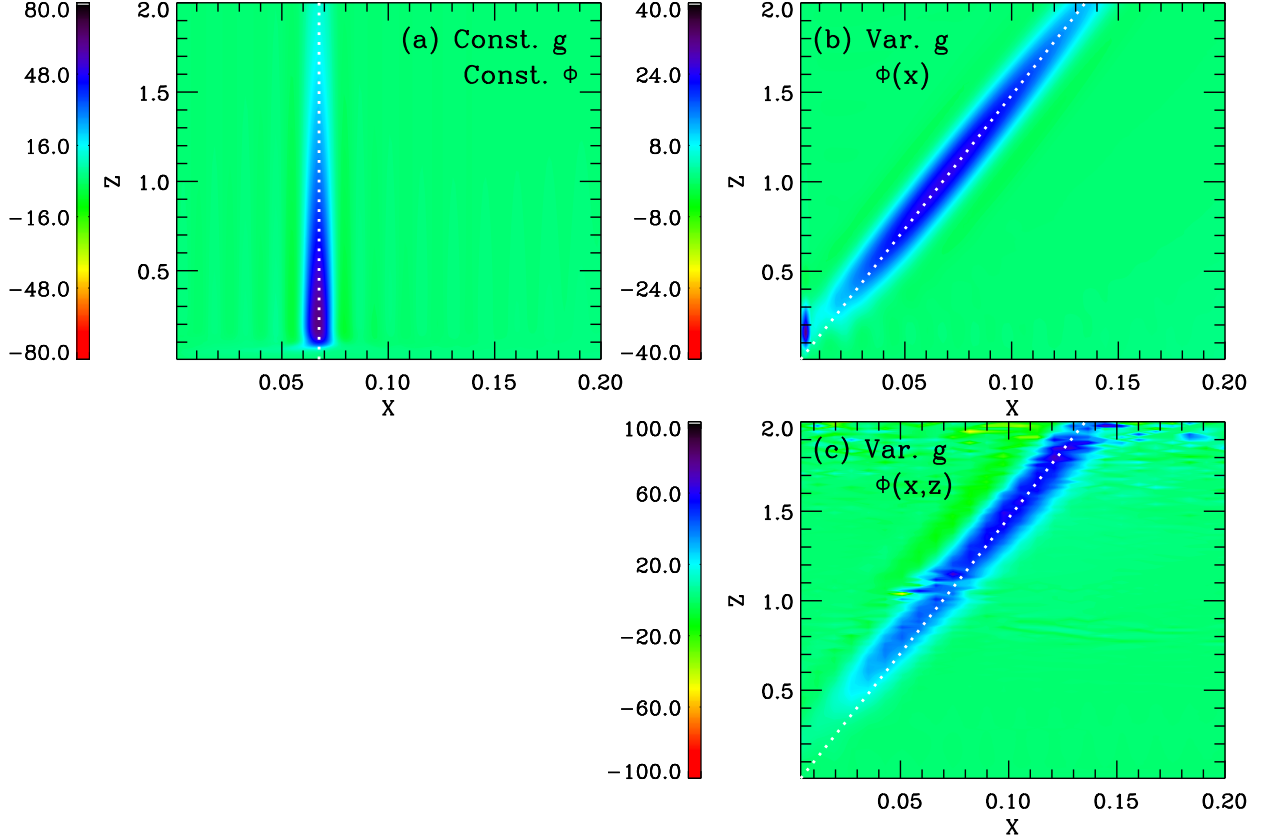


Fig. 1.— y -integrated torque density in the $x-z$ plane obtained from nonlinear numerical Athena simulations for $k_y h = 2\pi$ and $\gamma = 5/3$ for the three cases described in Section 3.1. The torque density $\partial_X \partial_Z T(X, Z)$ is scaled by $r^2 h \rho_{00} \Phi^2(X, Z)/c^2$ for $X = x/h$ (a different X from that in Fig. 2) and $Z = z/h$ (see equation (25)). Panel (a) is the case of constant gravity and simplified potential given by equation (24) that is independent of x and z . Panel (b) is the case of vertically varying gravity and simplified potential that is independent of z . Panel (c) is the case of vertically varying gravity and the potential is the k_y Fourier component of the planet potential. The artifact within $x < 0.005h$ of Panel (b) is due to the singularity in the cylindrical potential and the small smoothing length $5 \times 10^{-3}h$. The potentials are chosen to be weak enough to prevent gap opening. In all cases, the torque is confined to a thin region near the plane of the buoyancy resonance location (dotted line) defined by equation (9).

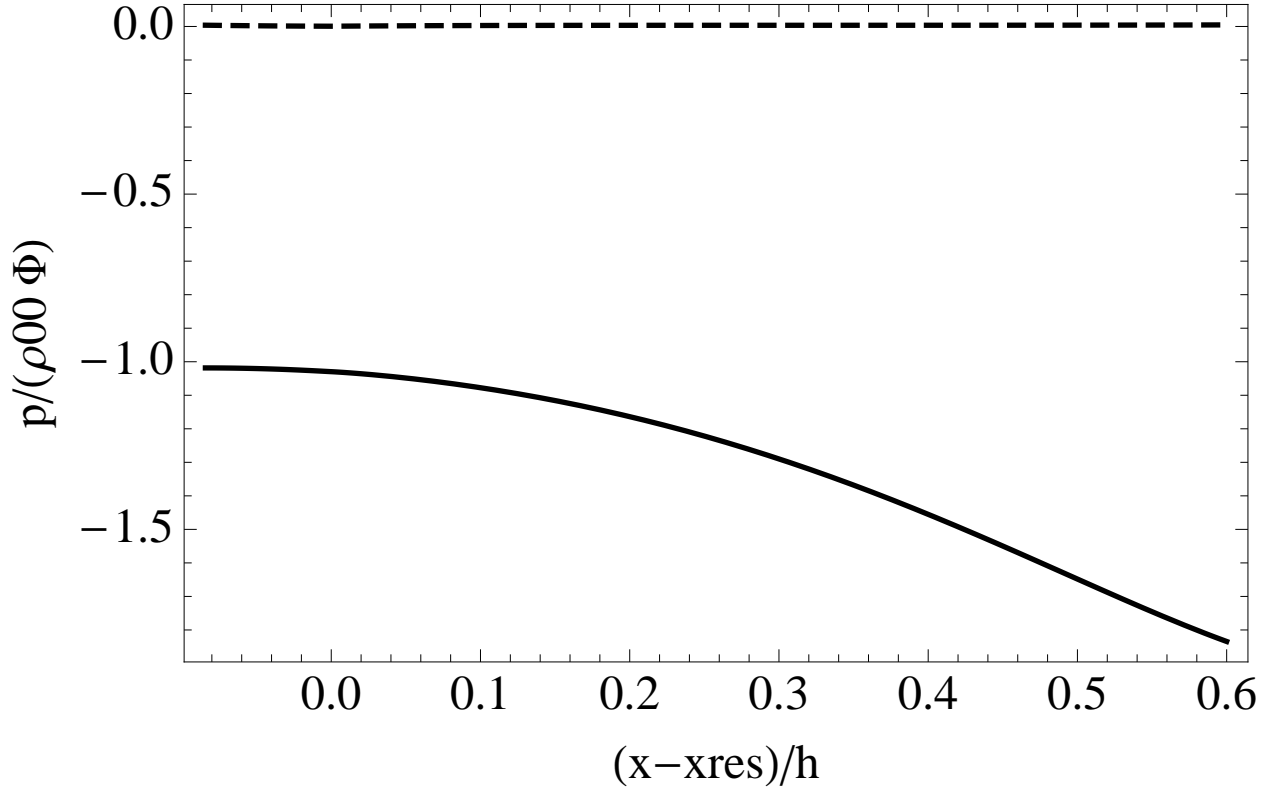


Fig. 2.— Numerical solution of equation (A4) for the dimensionless pressure perturbation $P(X) = p(X)/(\rho_{00}\Phi)$ as a function of position $X = (x - x_{\text{res}})/h$ relative to an outer buoyancy resonance. We take $K_y = k_y h = 5$ and $\gamma = 5/3$. We apply the x boundary conditions of Section 2.2 with inner boundary located at $x = 0$ and the outer boundary at $x = 0.6h + x_{\text{res}}$. The solid (dashed) line is the real (imaginary) part of P . Notice that $p \simeq -\rho_{00}\Phi$ near the resonance ($X = 0$), in agreement with the hydrostatic approximation of equation (26) and the series solution (A10) for large K_y . The resonance was resolved with $\epsilon = 1 \times 10^{-8}$.

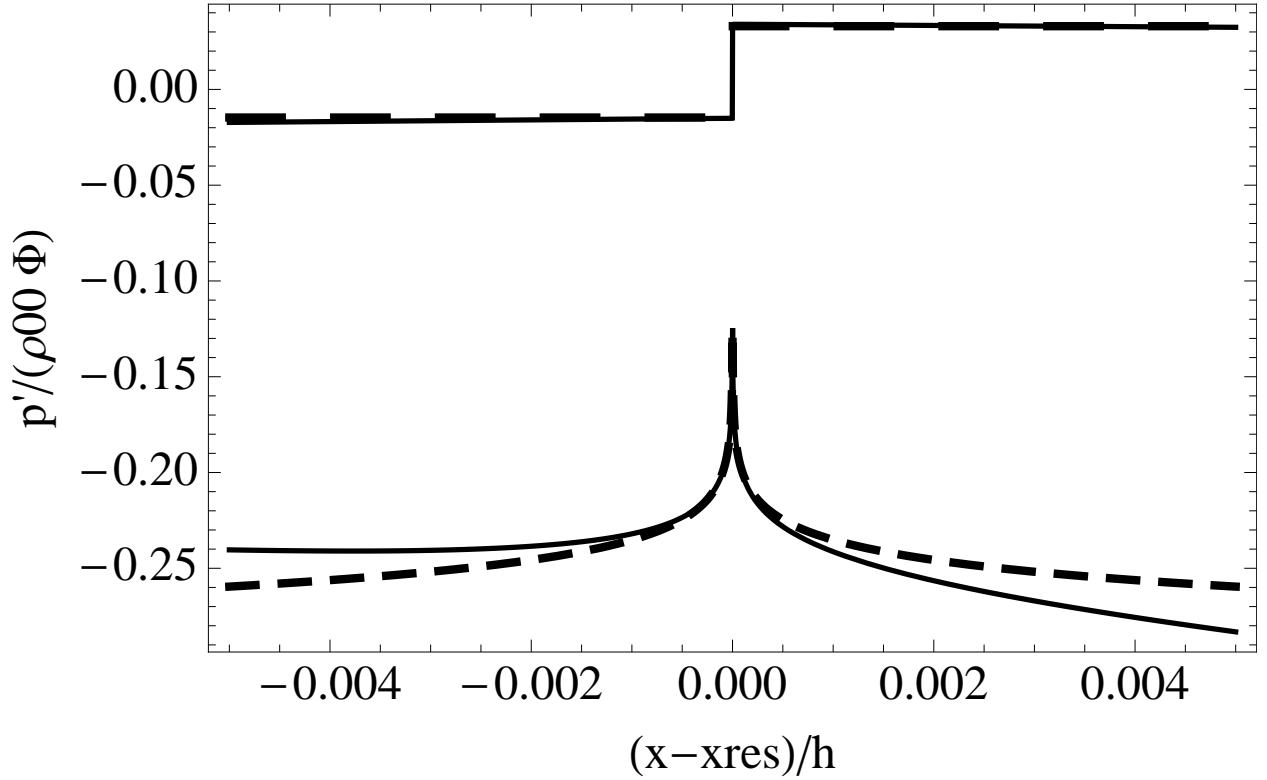


Fig. 3.— Numerical solution for the dimensionless first derivative of the pressure perturbation $P(X)$ as a function of X for the case described in Figure 2. The upper (lower) solid line plots the imaginary (real) part of $P'(X)$. The upper (lower) dashed line plots the imaginary (real) part of the analytic solution near the resonance given by equation (A15), together with equations (A14) and (A16), and $d_1 = -0.325 + 0.033i$.

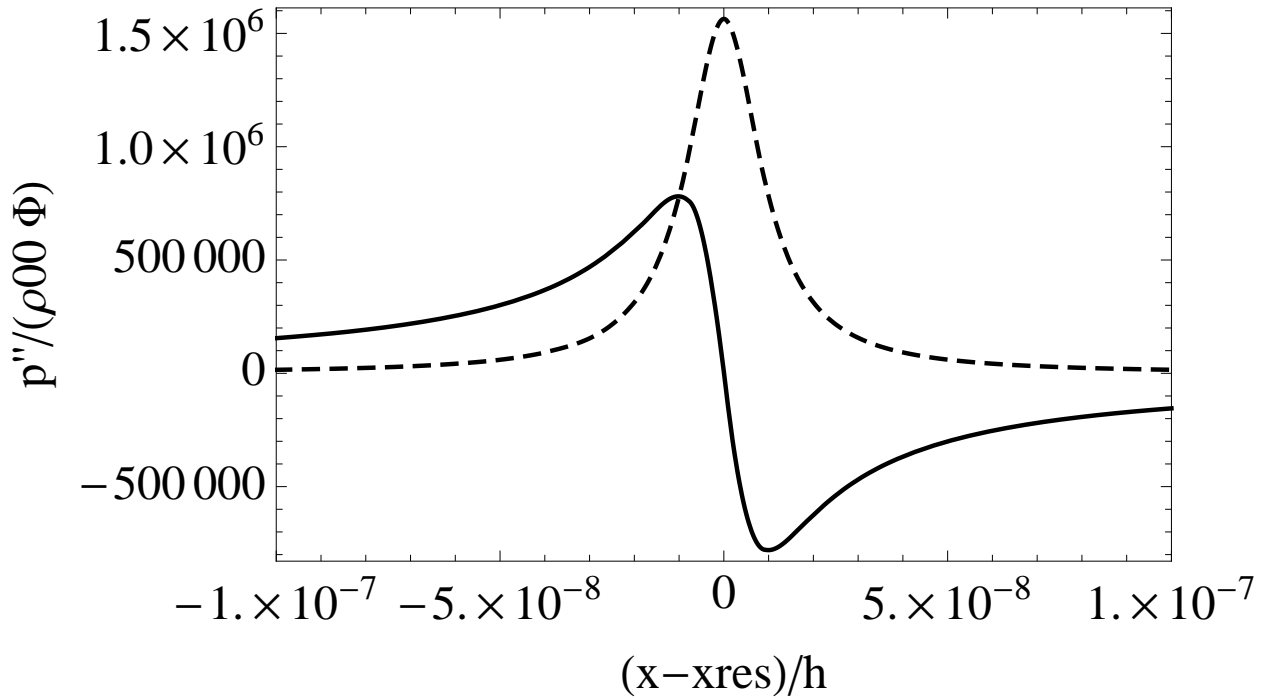


Fig. 4.— Numerical solution for dimensionless second derivative of the pressure perturbation $P(X)$ as a function of X for the case described in Figure 2. The solid (dashed) line is the real (imaginary) part of $P''(X)$. The resonance was resolved with a damping parameter $\epsilon = 1 \times 10^{-8}$ that determines the X scale of the curves, as discussed in Section 3.2.

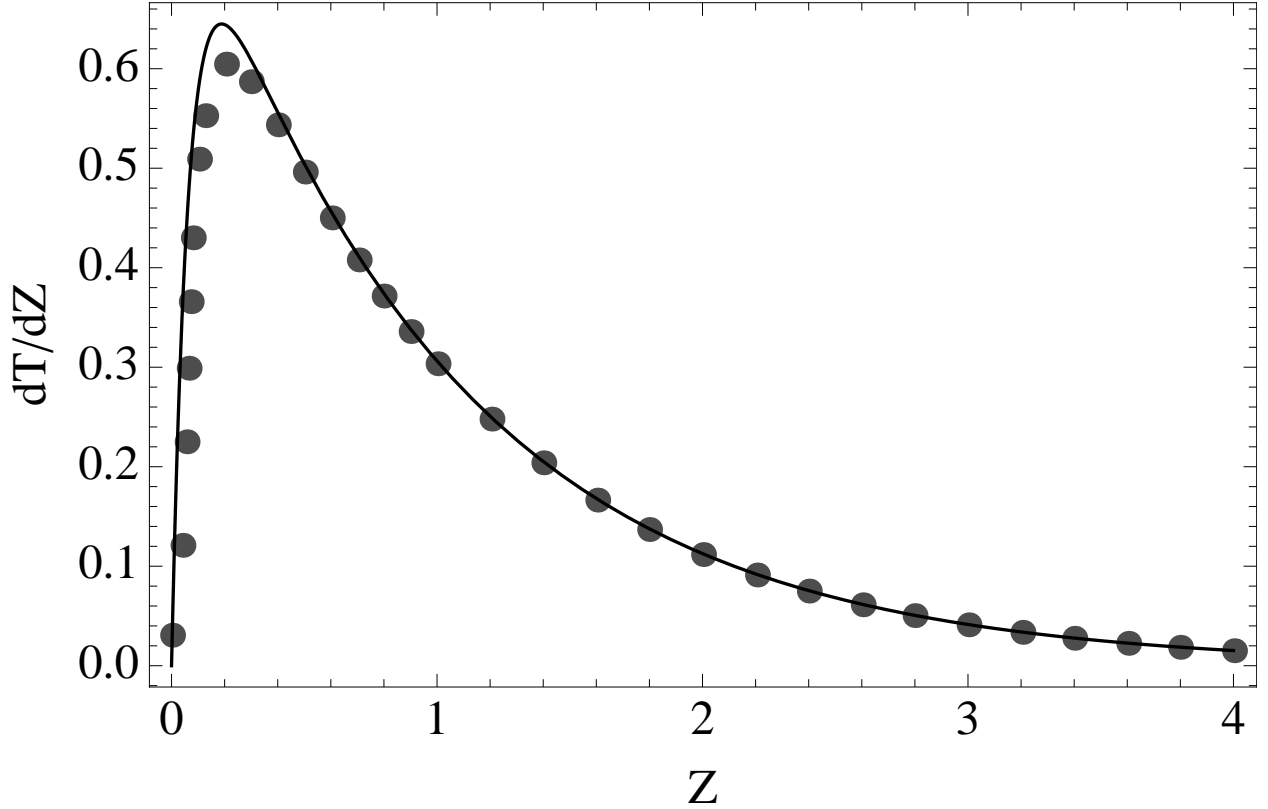


Fig. 5.— Dimensionless torque density distribution dT/dZ , normalized by $r^2 h \rho_{00} \Phi^2 / c^2$, at an outer buoyancy resonance as a function of height above the disk midplane $Z = z/h$ for Case (a) described in Section 3.1 that has constant vertical gravity and simplified potential. The line plots the analytic expression (B5) and the dots are the results of 3D nonlinear shearing box simulations with the Athena code that are evaluated through equation (39).

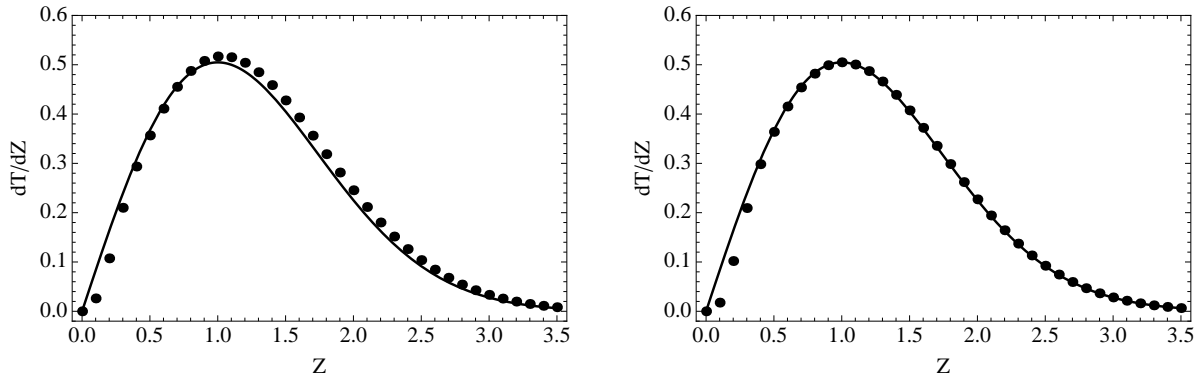


Fig. 6.— Torque density distribution dT/dZ normalized by $r^2 h \rho_{00} \Phi^2 / c^2$ at an outer buoyancy resonance as a function of height above the disk midplane $Z = z/h$ for models with $k_y h = 5$ (left panel) and $k_y h = 10$ (right panel). The vertical gravity varies linearly with z and the perturbing potential is given by equation (24). The line plots analytic expression (45) and the dots are the results of numerical linear 3D shearing box calculations that are based on a Fourier method in x described in Appendix C.